# Modelling and identification of characteristic intensity variations

Karl Rohr

*An approach is introduced for the modelling and identification of a certain class of characteristic intensity variations resulting essentially from polygonal structures of a depicted 3D-scene. We develop a general analytical model for the structural grey-value transitions in an image which is the superposition of elementary model functions. Special cases of this general model are the grey-value variations of step edges, grey-value corners (L-junctions), T-, Y-, ARROW-junctions, and all other junction types represented in the labelling system of Waltz[1]. It will be shown that this parametric model agrees fairly well with real image intensities. Estimates of the unknown model parameters are found by minimizing the sum of squared differences between the model and the observed grey values. The approach has been tested on real image data.*

*Keywords: model-based recognition, corners, junctions*

## MOTIVATION

The robust and precise recognition of characteristic (or prominent) intensity variations, such as grey-value corners and T-junctions, is important both for the visual perception of humans and for the automatic interpretation of images by computers. The more robustly and precisely those structures are derived from images, the more reliably can objects in the 3D-scene be described and recognized, and the 3D-scene be reconstructed.

Although many image analysis algorithms use prominent features as picture domain cues, there are hardly any detailed investigations of the behaviour of grey-value transitions in the vicinity of such two-dimensional grey-value structures[2]. It is well known that edge detectors incorporating the (implicit or explicit) assumption of one-dimensional grey-value transitions (e.g. Canny[3]) have difficulties when the grey-value structure under consideration has variations in two dimensions (see, for example, Li *et al.*[4]). In many cases, the detected edge contours are interrupted at such positions. Especially these image features with high content of information are in general poorly recovered. Often, rather heuristic approaches are used in a subsequent step to fill in missing contour points. Local operators for recovering two-dimensional intensity variations in many cases fail to infer the actual structure. To overcome this problem Lowe[5], for example, suggests a global search as opposed to local operations in the neighbourhood of each potential corner, i.e. to combine local and global information to recover characteristic intensity variations. Another problem arises from the usage of a Gaussian filter for noise reduction. Depending on the width of the filter, the blurring of the grey-value image leads in general to a displacement of the prominent structures (in some cases structures can disappear or new structures can even be created – see Damon[6]). To cope with the tradeoff between noise reduction and localization, one can take into account the dependency of the displacement on the width of the filter (see, for instance, Bergholm[7,8]). This can hardly be done without an explicit model of the characteristic grey-value structures.

In order to treat the problems mentioned above, we introduce in this contribution a model-based approach to recognize a certain class of characteristic grey-value variations. This class of grey-value transitions can be characterized in the image by several regions of constant image intensities joining in one prominent point, where the contours (grey-value edges) of the adjacent regions meet. It is supposed that the grey-value edges of such junctions are approximately straight lines in the vicinity of this point, i.e. the image intensities represent essentially polygonal structures of the scene. Furthermore, we assume symmetric grey-value transitions between two adjacent regions. This means that the grey-value transitions are (approximately) symmetric with respect to the line of steepest slope (locus of points where the gradient is maximal).

Institut für Algorithmen und Kognitive Systeme, Fakultät für Informatik der Universität Karlsruhe (TH), Postfach 6980, 7500 Karlsruhe 1, Germany

*Paper received: 31 August 1990; revised paper received: 17 April 1991*

0262–8856/92/002066–11 

We also assume the prominent grey-value variations to be represented by a sufficiently large number of pixels. This implies a picture function of sufficient resolution. The considered grey-value structures should also be well isolated, so that no interaction effects from other features take place. Specularities in the image are not considered in the present contribution. It seems that the assumptions we make are very restrictive. However, most existing approaches make implicitly use of them producing inaccurate results when the assumptions are not met in the image.

In order to model the proposed class of grey-value transitions, we develop a general analytical model. It will be shown that the structural grey-value variations of step edges, grey-value corners (L-junctions) T-, Y-, ARROW-junctions and all other junction types represented in the labelling system of Waltz[1], which is an expansion of the labelling system developed by Clowes[9] and Huffman[10], are special cases of this general parametric model. The model will be used for identification, that is for the precise recognition of essential properties of characteristic intensity variations in the image.

## RELATED LITERATURE

Examples of characteristic grey-value variations are grey-value corners (L-junctions; see, for example, Nagel[11]). In the present paper, the term *grey-value corner* denotes the grey-value transitions in a sufficiently large area around the prominent point of the grey-value corner. This grey-value corner point is usually defined as the point of maximal planar curvature in the line of steepest grey-value slope. Corner detection can simply mean to localize this prominent point or can, in addition, include the determination of inherent attributes. For this task, different methods are described in the literature. One can distinguish between direct and indirect methods. Indirect methods first detect edge points in the image. Then the corner point is taken to be the point of intersection of straight lines fit to edge points. Alternatively, the corner points are identified with local curvature extrema on a contour chain. Methods operating directly on images define the corner point as local maxima of values, determined either by combinations of partial derivatives of the picture function (e.g. see References 12–15), or by applying other masks directly on the image intensities (e.g. see References 16 and 17). In most approaches there is an underlying (implicit or explicit) model of the grey-value corner.

In order to illustrate why it is difficult to compute a description of an image with measurements that are not directionally selective, Marr[18] uses a 'corner-shaped' mask with aperture of 90°. The model we propose can be adapted to real corners appearing in any arbitrary orientation and is therefore, in the sense of Marr[18], directionally selective.

Bergholm[7] locates edges by tracking edge points from coarse to fine resolution along the direction in which they are displaced when blurred with Gaussian masks of different width. He uses an explicit model of grey-value corners (L-junction) to evaluate the displacement of the corner point depending on the mask size. This model is the convolution of an ideal wedge-shaped structure (characterized by the aperture of the sector and the height of the wedge) with a Gaussian function. The analytical corner model is similar to that of Berzins[19], who employed his model to analyse the accuracy of Laplacian edge detectors. The results of Bergholm[7] are superior with respect to Canny[3]. However, in the vicinity of grey-value corners and T-junctions, for example, there are still gaps. Thus, junctions are not recovered as desired. In the present contribution we use a similar mathematical model for grey-value corners to Berzins[19] and Bergholm[7]. We compare this model directly with the observed image intensities to adapt the model to individual grey-value structures. The result of this process provides not only an estimate for the position of the corner point, but also determines all other parameters characterizing the corner model. Even if the image is smoothed to reduce the noise, an estimate of the position of the corner point in the unblurred image is found without explicit tracking.

In order to derive a corner detector, Rangarajan *et al.*[17] extend the approach of Canny[3] for detecting one-dimensional grey-value transitions to two dimensional features. They derive two functions, one describing the corner detector inside and the other outside the sector of the underlying corner model. Contrary to Rangarajan *et al.*[17], in the present contribution the analytical description for recognizing grey-value corners consists of just one function which characterizes the whole area around the corner point. By choosing suitable model parameters, all corners belonging to the proposed class can be modelled.

Guiducci[20] characterizes corners by three parameters: amplitude, aperture and smoothness of the ideal wedge. Based on the grey-value corner characterization of Dreschler and Nagel[12] he derives analytical expressions for these three parameters to estimate them from image data. In the present paper we introduce a grey-value corner model which is characterized by seven parameters: position of the corner point (2); orientation (1); aperture (1); intensities of the grey-value plateaus (2); and the strength of the blurring by a Gaussian function (1). All seven parameters are determined by fitting this parametric model to the observed image intensities. By this, we have a measure of how well the estimated model approximates the actual data. All parameters are assigned real numbers. So the position of the corner point is determined to subpixel accuracy and indicates the origin of the ideal (unsmoothed) grey-value structure. Moreover, this model is a special case of a more general model for characteristic grey-value structures introduced in the next section.

## MODELLING OF CHARACTERISTIC INTENSITY VARIATIONS

A digital picture, recorded by an imaging sensor, is not only disturbed by noise but is also band-limited in the frequency range. Due to the recording process, sharp transitions (e.g. step edges) are rounded-off and corrupted by noise. In order to reduce the noise one can apply a Gaussian filter. The advantages of such an operation are described elsewhere (see, for example, Marr and Hildreth[21]). However, the application of a

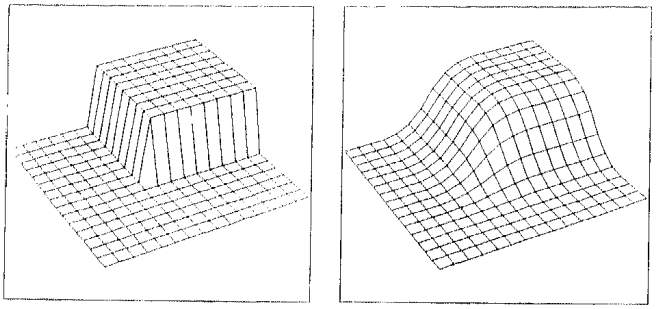

*Figure 1 (left). Wedge shaped grey-value structure (ideal grey-value corner)*

*Figure 2 (right). Grey-value corner model*

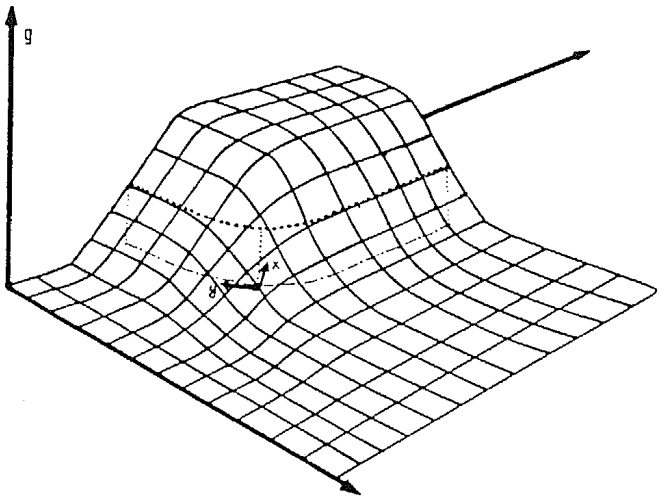


*Figure 3. Grey-value corner as proposed by Nagel[11]*

Gaussian filter smooths both the noise and the structural intensity variations. The blurring leads to a further rounding-off of the original sharp transitions. If the signal-to-noise ratio is large, the blurred step edge can be interpreted as an ideal sharp step edge convolved with a Gaussian filter. We can also extend this interpretation to other grey-value transitions in the image.

## Experimental model

Analogously to the modelling of a step edge described above, a grey-value corner (L-junction) can be modelled by convolution of a wedge shaped structure (ideal grey-value corner, 'piece of cake') shown in Figure 1 with a two-dimensional Gaussian function (see Figure 2). The aperture of the wedge in this example is 90°. The size of the Gaussian filter, specified by the parameter $\sigma$, determines the smoothness of the blurred wedge. Comparison of Figure 2 with the qualitative model of Nagel[11], depicted in Figure 3, shows that the two models agree (see also Dreschler[22]).

Similarly to modelling step edges and grey-value corners, we can model intensity variations consisting of three adjacent regions. Figure 5 shows a T-junction obtained by convolution of the structure in Figure 4 with a Gaussian filter. If we compare this synthetic T-junction with a real T-junction (Figure 7 is the original image and Figure 8 shows the 3D-plot belonging to this T-junction), or with the blurred version in Figure 9, we see that the structures are very similar. In addition, Figure 8 suggests that the structural grey-

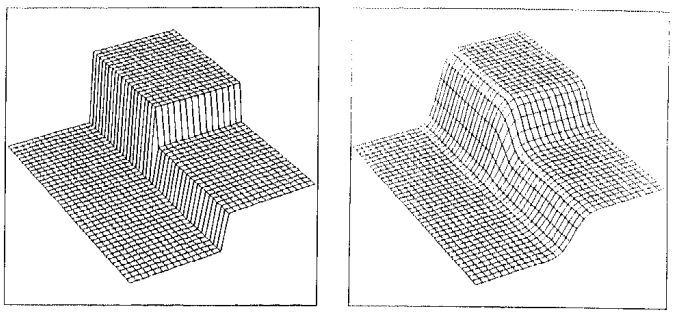

*Figure 4 (left). Ideal T-junction*

*Figure 5 (right). Blurred ideal T-junction of Figure 4*

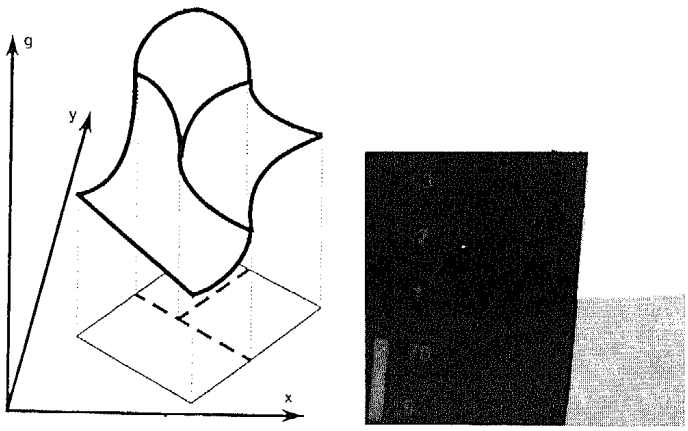


*Figure 6 (left). Sketch of a continuous T-junction by Nagel[23]*

*Figure 7 (right). Real T-junction*

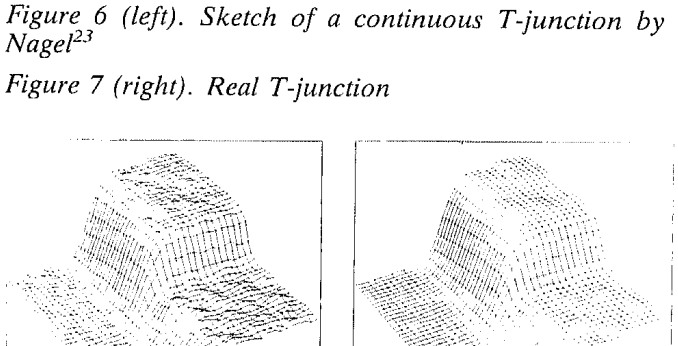

*Figure 8 (left). 3D-plot of the T-junction in Figure 7*

*Figure 9 (right). Blurred real T-junction of Figure 8*

value variations of this T-junction are more suitably described by a continuous function than by discrete description elements. The qualitative behaviour of this real T-junction agrees with the sketch of a continuous T-junction in Nagel[23] (see Figure 6).

By superposition of a number $n$ of wedge shaped structures like in Figure 1 (with arbitrary aperture and intensity) and subsequent Gaussian filtering, we can model arbitrarily complex structures of the proposed class of grey-value structures. The models can be created in any orientation by carrying out an additional rotation.

## Analytical model

In the preceding section, the grey-value structures were modelled by two separate steps: composition of ideal

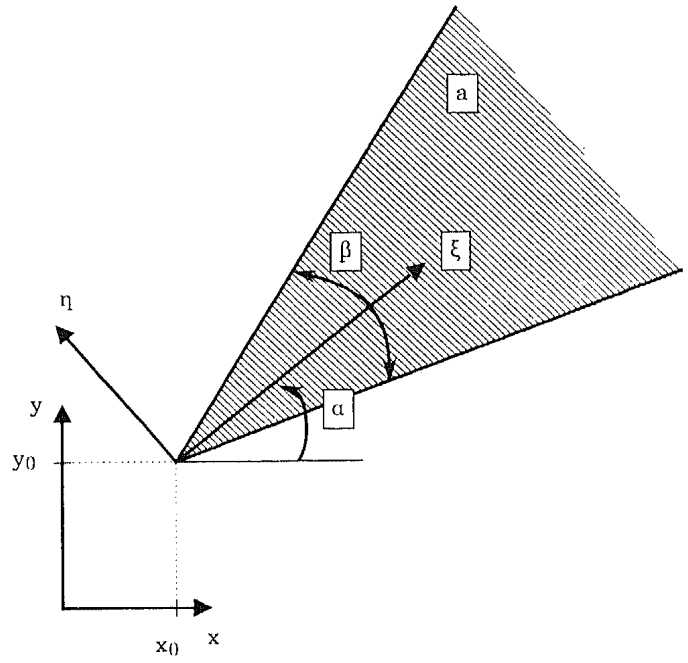


a0

*Figure 10. Grey-value corner in the absolute coordinate system*

wedge shaped structures, and subsequent smoothing with a Gaussian filter. Indeed, these two steps can be combined by just one analytical function.

**Two adjacent regions (step edge, grey-value corner)**
An ideal grey-value corner $E(x, y)$ (wedge shaped structure) can be characterized, as shown in Figure 10, by three parameters: the aperture $\beta$, the amplitude $a$ and an angle of rotation $\alpha$ which denotes the orientation of $E(x, y)$ with respect to the $x$-axis. Let the local Cartesian coordinate system $(\xi, \eta)$ be aligned in such a way that the sector of the wedge is symmetric to the $\xi$-axis. Then this sector is divided into two parts with aperture $\beta/2$. Let the origin of the coordinate system (origin of the grey-value corner, corner point) be the point $(x_0, y_0)$. Convolution of $E(x, y)$ with a two-dimensional Gaussian function $G(x, y)$ results in the model of a grey-value corner (L-junction) given by $g_{ML}(x, y) = g_{ML}(x, y, x_0, y_0, \alpha, \beta, a, \sigma)$:

$$g_{ML}(x, y) = E(x, y) * G(x, y) = \int_{-\infty}^{+\infty}\int_{-\infty}^{+\infty} E(\xi, \eta)\, G(x-\xi, y-\eta)\, d\xi\, d\eta \quad (1)$$

In the following we derive an analytical expression for $g_{ML}(x, y, \beta, a, \sigma)$, that means we consider the problem in the local coordinate system $(x_0 = y_0 = \alpha = 0)$. The grey-value corner in the absolute coordinate system $g_{ML}(x, y, x_0, y_0, \alpha, \beta, a, \sigma)$ can then be evaluated by an additional translation $(x_0, y_0)$ and a rotation about an angle $\alpha$. With:

$$G(x) = \frac{1}{\sqrt{2\pi}} e^{-(x^2/2)} \qquad G(x, y) = G(x)\, G(y)$$

and $t = \tan(\beta/2)$ we hence obtain for the upper part of the sector:

$$M(x, y, \beta) = \int_{\xi=0}^{\infty}\int_{\eta=0}^{t\xi} G(x-\xi, y-\eta)\, d\xi\, d\eta$$

Integration of $G(x)$ yields the Gaussian error function $\phi(x)$. Using:

$$\phi(x) = \int_{-\infty}^{x} G(\xi)\, d\xi \quad \phi(x, y) = \phi(x)\, \phi(y)$$

$$D(x, y) = G(x)\, \phi(y)$$

it follows that:

$$M(x, y, \beta) = \phi(x, y) - \int_{-\infty}^{x} D(\xi, t(\xi - x) + y)\, d\xi \quad (2)$$

The lower part of the sector is just a reflection with respect to the $x$-axis. So the model function of the whole sector can be obtained by superposition of two model functions in (2):

$$g_{ML}(x, y, \beta, a, \sigma) = a\left(M\left(\frac{x}{\sigma}, \frac{y}{\sigma}, \beta\right) + M\left(\frac{x}{\sigma}, -\frac{y}{\sigma}, \beta\right)\right) \quad (3)$$

We use the formulation in (3) for describing the intensity variations of an L-junction because this function is valid for angles in the whole range of $0° \leq \beta < 180°$. Moreover, more complex junctions (see below) can again be obtained by superposition of this function. The construction of grey-value structures by superposition of model functions is possible because the convolution with a Gaussian function is a linear operation, and linear operations satisfy the superposition principle[24]. The whole grey-value structure can be decomposed into several elementary components (in our case wedge shaped structures) in such a way that the result of an operation (in our case the convolution with a Gaussian function) can 'easily' be calculated. The result of the operation onto the whole structure is then the composition of the results obtained for the elementary components.

In order to compute function values of $g_{ML}(x, y)$, we chose Romberg's method[25] for numerical integration using rational approximations of the $\phi$-function in Abramowitz and Stegun[26]. The employed limits of integration can be obtained by estimating the integrand of (2). Because the $\phi$-function is monotonically increasing from 0 to 1 the integrand is surely smaller than or equal to $\epsilon$ if $G(\xi) \leq \epsilon$, i.e. $|\xi| \geq \sqrt{-2\ln(\sqrt{2\pi}\epsilon)}$. A synthetic image of a grey-value corner can now be created by superposition of the model function $g_{ML}(x, y)$ with a surface of constant intensity $a_0$. However, we can also imagine this complete grey-value structure as the superposition of two model functions with aperture $\beta$ and $360°-\beta$:

$$\begin{aligned} g_{ML}(x, y, x_0, y_0, \alpha, \beta, a_0, a, \sigma) &= g_{ML_1}(x, y) + g_{ML_2}(x, y) \\ &= g_{ML}(x, y, x_0, y_0, \alpha, \beta, a, \sigma) \\ &\quad + g_{ML}(x, y, x_0, y_0, \alpha + 180°, 360° - \beta, a_0, \sigma) \end{aligned} \quad (4)$$

Equation (3) is valid for $0° \leq \beta < 180°$. The choice $\beta = 180°$ defines the model of a step edge:

$$g_{MSK}(x, y, a, \sigma) = a\phi\left(\frac{x}{\sigma}\right)$$

If $\beta > 180°$ then $g_{ML}(x, y)$ can be computed using two model functions with half of the aperture and same intensity or by superposition of $g_{MSK}(x, y)$ and $g_{ML}(x, y)$. Thus, general intensity variations of two adjacent regions of the proposed class of grey-value structures, which will be denoted by $g_{M2}(x, y)$, can be created using the model function of the step edge $g_{MSK}(x, y)$ and the L-junction $g_{ML}(x, y)$. In the general case, the grey-value structures are specified by seven parameters:

$$g_{M2}(x, y) = \sum_{i=1}^{2} g_{MLi}(x, y) \quad \text{with}$$

$$g_{ML}(x, y) = \begin{cases} g_{MSK}(x, y) & \text{if } \beta = 180° \\ g_{ML}(x, y) & \text{if } \beta \neq 180° \end{cases}$$

**Three adjacent regions (T-, Y-, *ARROW*-Junction)**
Grey-value variations which are characterized by three plateaus of constant intensities joining in one point can also be modelled by superposition of model functions $g_{ML}(x, y)$. One possible parametrization of the image of a trihedral vertex is sketched in Figure 11. Each wedge is described by an angle of rotation, an aperture and an amplitude. Because the angle of rotation of the second sector $\alpha_2$ can be expressed by $\alpha_2 = \alpha_1 - \beta_1/2 - \beta_2/2$, the number of parameters characterizing such a grey-value structure is 9. Analogously to the realization of synthetic grey-value corners, we can model the intensity variations of three adjacent regions $g_{M3}(x, y)$ by the superposition of two model functions $g_{ML}(x, y)$ and one plateau of constant intensities. Likewise, we can create such a grey-value structure by superposing three model functions $g_{ML}(x, y)$:

$$\begin{aligned} g_{M3}(x, y, x_0, y_0, \alpha, \beta_1, \beta_2, a_0, a_1, a_2, \sigma) \\ &= \sum_{i=1}^{3} g_{MLi}(x, y) \\ &= g_{ML}(x, y, x_0, y_0, \alpha, \beta_1, a_1, \sigma) + \\ &\quad g_{ML}(x, y, x_0, y_0, \alpha - \beta_1/2 - \beta_2/2, \beta_2, a_2, \\ &\quad \sigma) + g_{ML}(x, y, x_0, y_0, 180° + \alpha - \beta_2/2, \\ &\quad 360° - \beta_1 - \beta_2, a_0, \sigma) \end{aligned} \tag{5}$$

Particular choices of the parameters of $g_{M3}(x, y)$ yield the grey-value variations of a T-, Y- or ARROW-junction. The T-junction is specified by $\beta_1 + \beta_2 = 180°$. A Y- and ARROW-junction is given by $\beta_1 + \beta_2 > 180°$ and $\beta_1 + \beta_2 < 180°$, respectively, if $\beta_1$ and $\beta_2$ are the two smaller angles. The model of the Y-junction proposed in De Micheli *et al.*[27] is a special case of (5) if we choose, for example, $x_0 = y_0 = 0$, $\alpha = 90°$, $\beta_1 = 180° - 2\theta$, $\beta_2 = 90° + \theta$, $a_0 = A$, $a_1 = 0$ and $a_2 = B$. In De Micheli *et al.*[27], this model is employed to compare existing edge detection algorithms according to their accuracy of localization and sensitivity to noise.

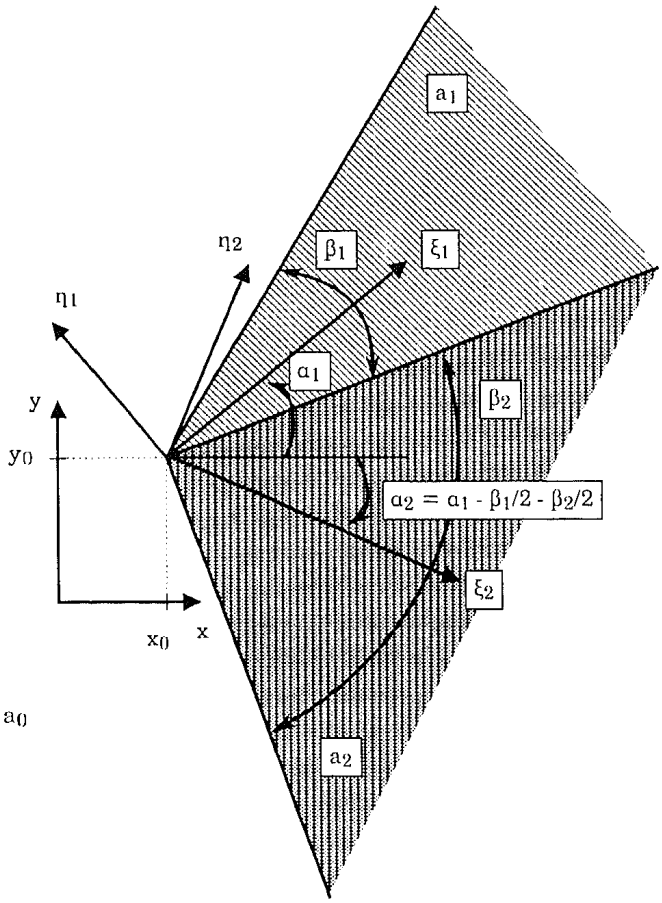

*Figure 11. Three adjacent regions*

**$n$ adjacent regions**
The validity of the superposition principle is the reason why we can model grey-value structures by superimposing an arbitrary number $n$ of wedge shaped structures (elementary components). Conversely, we can derive from the general case of $n$ adjacent regions $g_{Mn}(x, y)$ the grey-value structures for $n = 2$ and $n = 3$ introduced in the preceding sections:

$$\begin{aligned} g_{Mn}(x, y) &= \left(\sum_{i=1}^{n} E_i(x, y)\right) * G(x, y) \\ &= \sum_{i=1}^{n} (E_i(x, y) * G(x, y)) \\ &= \sum_{i=1}^{n} g_{MLi}(x, y) \quad n \geq 2 \end{aligned} \tag{6}$$

The choice $n = 2$ specifies the intensity variations of a step edge or a L-junction. For $n = 3$ we obtain T-, Y- and ARROW-junctions. In the case of $n = 4$ we have PEAK-, K-, X-, MULTI- and XX-junctions in the notation of the labelling system of Waltz[1]. For $n = 5$ we have KA- and KX-junctions, and $n \geq 6$ leads to even more complex grey-value structures. The specific number of model parameters is $m = 3 + 2n$. For illustration the 3D-plot of a K-junction is depicted in Figure 12.

## IDENTIFICATION OF CHARACTERISTIC INTENSITY VARIATIONS

The aim of identification is to find a suitable description

for a real object. The task is to determine a mathematical model which reflects the essential properties of the real object sufficiently well[28,29]. First it is necessary to select a certain model class, and second to choose a representative of this class by fixing the model parameters. The model class is chosen by using *a priori* knowledge, and the estimation of the parameters takes into account current empirical observations (measurements). For the identification of grey-value variations in images, i.e. the precise recognition of grey-value structures with respect to their characteristics, the analytical model introduced above is selected as model class. Let us simplify the notation by denoting the image plane coordinates with $\boldsymbol{x} = (x, y)$ and the model parameters we wish to estimate with $\boldsymbol{p} = (p_1, \ldots, p_m)$. The function $g_M(\boldsymbol{x}, \boldsymbol{p})$, the model description, should be chosen in such a way that the agreement with the grey values in the image $g(\boldsymbol{x})$ is as close as possible. We require the sum of the squared differences between the model function and the grey values in an area $\Omega$ around the origin of the grey-value structure to be as small as possible. Then the nonlinear cost function $S$ depending on the parameters $\boldsymbol{p}$ is as follows:

$$S(\boldsymbol{p}) = \int_{\Omega} (g_M(\boldsymbol{x}, \boldsymbol{p}) - g(\boldsymbol{x}))^2 \, d\boldsymbol{x} \rightarrow \min \tag{7}$$

and one discrete version of the above is:

$$S(\boldsymbol{p}) = \sum_i (g_M(\boldsymbol{x}_i, \boldsymbol{p}) - g(\boldsymbol{x}_i))^2 \rightarrow \min \tag{8}$$

We search the values for $\boldsymbol{p}$ where $S(\boldsymbol{p})$ takes a (local) minimum. In order to get first experimental results we use the descent method of Powell[30]. Reducing the computation time will be the subject of future work. After choosing an initial starting vector $\boldsymbol{p}_0$, the iteration process proceeds until the differences of the values of the function $S(\boldsymbol{p})$ in subsequent iteration steps normalized by the absolute values of the function, drop below a predefined threshold.

## EXPERIMENTAL RESULTS

This section demonstrates the behaviour of the proposed method for real image data. We show identification results for the image depicted in Figure 13, which was recorded with a HDTV-camera ($1024 \times 1024$ pixels) and the image in Figure 26 taken with an ordinary camera ($512 \times 512$ pixels). The considered features are marked in Figures 15 and 28. Preliminary results are described by Rohr[31].

### Initial values for the optimization process

The initial values $\boldsymbol{p}_0$ needed for the optimization process should be chosen automatically. One possibility is to construct prototypes, representing certain grey-value variations, by using the analytical model outlined above. By applying these prototypes we would get a rough indication of the individual grey-value structure being observed. The analysis of the grey-value variations could then be refined by the proposed identification approach. Here, we suggest another possibility. Initial values for the position of the grey-value structures are determined by applying the approach of

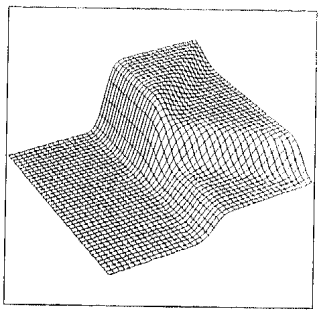

*Figure 12 (left). 3D-plot of an analytical K-junction*

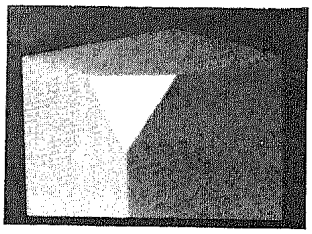

*Figure 13 (right). Original image of a cut cube*

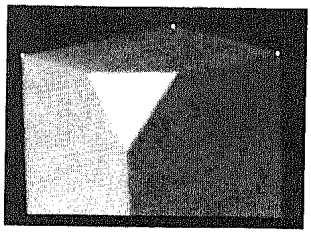

*Figure 14 (left). Detected features of Figure 13*

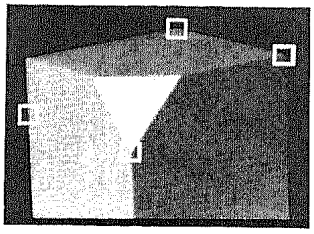

*Figure 15 (right). Considered features of Figure 13*

Rohr[32] which detects image points indicating high intensity variations. This local approach operates directly on the image utilizing the matrix $\underline{C}$ suggested in Nagel[33]. The elements of $\underline{C}$ are combinations of partial derivatives of the picture function. In Rohr[32] local maxima of the determinant of $\underline{C}$ are identified with points of high intensity variations. In order to suppress local maxima in homogeneous regions due to noise $det(\underline{C})$ is compared with a threshold. Edge points outside corners are removed using $det(\underline{C})/(\frac{1}{2}trace(\underline{C}))^2$ by Nagel and Enkelman[34]. After estimating the partial derivatives with $5 \times 5$-masks[35], the localization of the corner points are refined by applying $3 \times 3$-masks. Figure 14 shows the result of this approach for the image in Figure 13.

Initial values for the angles are evaluated using straight lines fit to linked edge points in the vicinity of the examined grey-value structure. Single edge points are localized by the approach of Korn[36]. The mean values of the intensities in the sectors (bounded by the straight lines) are taken as an estimate for the amplitude of the grey-value plateaus. For illustration we determine initial values for the Y-junction in Figure 16 appearing in the centre of the image shown in Figure 13. The initial position of this grey-value structure is marked by a square (see Figure 17). The straight lines indicate the boundaries of the sectors and the marked points inside the sectors contribute to the estimation of the mean values for the grey-value plateaus. Only those points are considered where $det(\underline{C})$ is smaller than a threshold.

### Identification results

We start with the identification of a step edge (see Figures 15 and 18). Because an edge point is only determined uniquely in one direction, i.e. the direction of the grey-value gradient belonging to it, we restrict the position of the edge point during the optimization

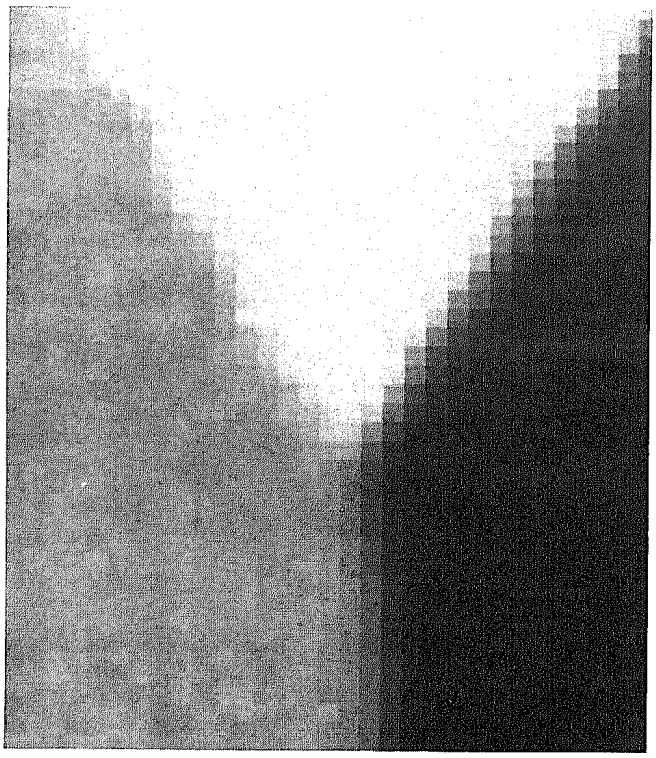

*Figure 16. Original image of a Y-junction*

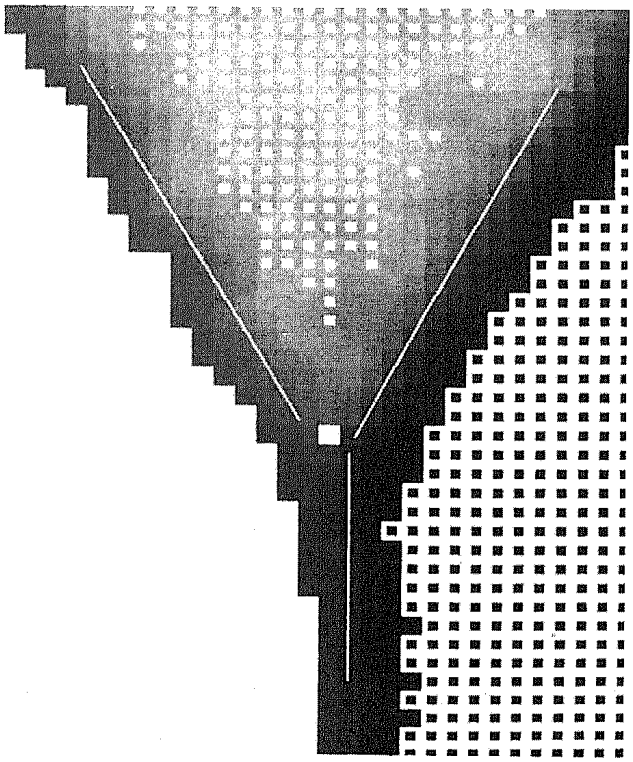

*Figure 17. Illustration of the initial data for the Y-junction in Figure 16: position, angles and grey values of the plateaus*

process by an add tional requirement. In our case, we can choose a certain row in the image (fixing the value of $y_0$). Then the number of the remaining unknown parameters is 5: ($x_0$, $\alpha$, $a_0$, $a$, $\sigma$). Applying the identification approach to a ca. $20 \times 20$ portion of the original image, we get the parameters shown in the first

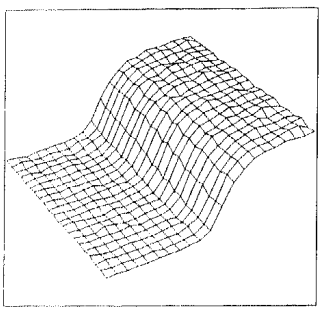

*Figure 18 (left). Original step edge*

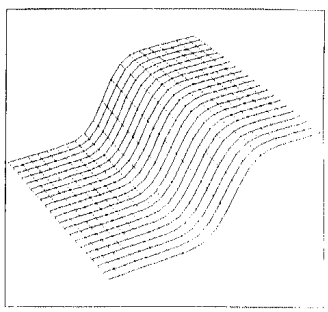

*Figure 19 (right). Identified model of the step edge in Figure 18*

**Table 1. Identification result of the step edge in Figure 18**

| $\sigma_F$ | $x_0$ | $\alpha$ | $a_0$ | $a$ | $\sigma$ | $\bar{e}$ | $\sigma_0$ |
|---|---|---|---|---|---|---|---|
| 0.0 | 11.87 | 3.87 | 16.15 | 115.09 | 1.52 | 2.48 | 1.52 |
| 0.5 | 11.87 | 3.97 | 16.13 | 114.92 | 1.59 | 1.98 | 1.51 |
| 1.0 | 11.86 | 4.27 | 16.25 | 114.03 | 1.82 | 1.02 | 1.52 |
| 1.5 | 11.89 | 4.24 | 16.08 | 114.66 | 2.13 | 0.60 | 1.52 |

row in Table 1. The mean error $\bar{e}$ (positive root of the mean squared error) between the original image and the model function is 2.48. The model function approximates the original step edge fairly well (see Figures 18 and 19). The estimated value for $\sigma$ is 1.52 and represents a measure for the width of the grey-value transition.

In order to reduce the noise we will now smooth the original image with a Gaussian filter $\sigma_F$ before applying the optimization method. For values $\sigma_F =$ 0.5, 1.0 and 1.5 we get the estimated parameters as shown in Table 1. The mean error $\bar{e}$ gets smaller with increasing $\sigma_F$. Obviously, the more we smooth the image beforehand the better is the agreement of the image with the model function. In addition, we see that the parameters, with exception of $\sigma$, remain nearly constant, i.e. they are (nearly) independent of $\sigma_F$. However, the changes of $\sigma$ are to be expected because filtering the image increases the width of the grey-value transitions. Imagine the original step edge to be a smoothed ideal step edge, then the filtered original step edge is the result of two Gaussian filters $\sigma_0$ (the optimal value for the unfiltered original image) and $\sigma_F$ applied successively to the ideal step edge. Equally, an ideal step edge can be smoothed with just one Gaussian filter of $\sigma = \sqrt{\sigma_0^2+\sigma_F^2}$. This is not only true for step edges but for arbitrary grey-value structures $g(\boldsymbol{x})$:

$$\begin{aligned}&[g(\boldsymbol{x}) * G(\boldsymbol{x}, \sigma_0)] * G(\boldsymbol{x}, \sigma_F)\\ &\quad = g(\boldsymbol{x}) * [G(\boldsymbol{x}, \sigma_0) * G(\boldsymbol{x}, \sigma_F)]\\ &\quad = g(\boldsymbol{x}) * G(\boldsymbol{x}, \sqrt{\sigma_0^2+\sigma_F^2})\end{aligned} \tag{9}$$

Thus, the width of a grey-value transition in the original image $\sigma_0$ can be evaluated using:

$$\sigma_0 = \sqrt{\sigma^2-\sigma_F^2} \tag{10}$$

If we now consider the values for $\sigma_0$ (last column in Table 1), we see that (10) is confirmed. Consequently,

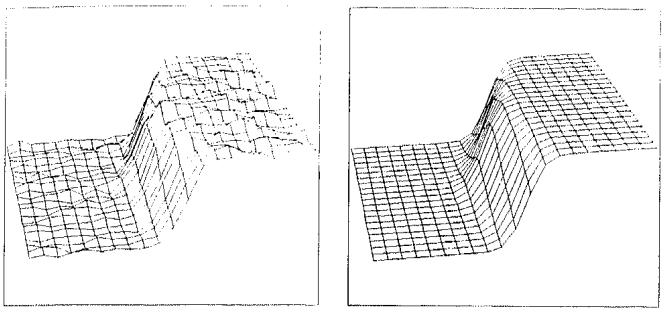

*Figure 20 (left). Original grey-value corner*

*Figure 21 (right). Identified model of the grey-value corner in Figure 20*

**Table 2. Identification result of the grey-value corner in Figure 20**

| $\sigma_F$ | $x_0$ | $y_0$ | $\alpha$ | $\beta$ | $a_0$ | $a$ | $\sigma$ | $\bar{e}$ | $\sigma_0$ |
|---|---|---|---|---|---|---|---|---|---|
| 0.0 | 27.18 | 28.60 | 267.72 | 158.33 | 15.33 | 64.12 | 0.96 | 1.60 | 0.96 |
| 0.5 | 27.22 | 28.64 | 267.63 | 159.17 | 15.32 | 64.01 | 1.09 | 1.03 | 0.97 |
| 1.0 | 27.24 | 28.50 | 267.82 | 159.65 | 15.35 | 63.87 | 1.42 | 0.43 | 1.01 |
| 1.5 | 27.23 | 28.39 | 267.96 | 159.34 | 15.30 | 63.95 | 1.78 | 0.26 | 0.96 |

all parameters are nearly independent of smoothing the original image beforehand. However, if the image is smoothed too much, the obtained parameters will be inaccurate. The position of the prominent point of the grey-value structure is determined (nearly) independently of the width of the grey-value structure and of the amount of filtering, because the estimated position is the origin of the grey-value structure, i.e. the position for the model parameter $\sigma = 0$. Hence, the influence of, for example, a badly focused camera or of different sharpness of the grey-value structures due to variations of the distances of objects in the scene to the camera is reduced. The application of the identification method for ideal synthetic images (sharp transitions and no noise) also yielded good results. The step edges were identified almost exactly. The mean error would be approximately zero. If, for example, the jump of the step edge was located between columns 9 and 10, then the optimal position of the identified model would be 9.5.

For some further tests of our approach on other images we refer to Bergholm and Rohr[37], where the estimates for the width and height of step edges were compared with the estimates of the approach of Zhang and Bergholm[38]. The comparison showed that the two different approaches (assuming the same step edge model) yield similar results if the step edge model is valid. If, however, the width of the transitions is large the approach described in the current contribution seems to be more precise.

Nalwa and Binford[39] also fit an explicit model to step edges. They use the *tanh*. However, they did not extend their approach to two-dimensional features such as grey-value corners and more complex junctions.

Next we want to identify the grey-value corner (see Figure 20) in the rear of the cube in Figure 13. The aperture of the sector is very big. Consequently, the recognition of this grey-value structure is difficult because the position of the corner point is not very well defined. The estimated model parameters $\boldsymbol{p}$ are shown in Table 2. The identified model is depicted in Figure 21. Similar to the example of the step edge, the deviation between the image and the model gets smaller with increasing values of $\sigma_F$. The obtained parameters are (nearly) independent of $\sigma_F$.

The identification result of the Y-junction in Figure 22 appearing in the middle of the image in Figure 13 is displayed in Figure 23. The values for the estimated parameter vectors $\boldsymbol{p}$ are presented in Table 3. Qualitatively, we recognize the same behaviour as for the step edge and the grey-value corner. For this more complex recognition problem, the parameters obtained are (nearly) independent of $\sigma_F$, too. The same holds for the identification of the ARROW-junction (see Figures 24 and 25, and Table 4).

We also show identification results for the image in Figure 26. The detected features can be seen in Figure 27. For the features marked in Figure 28 (L-, Y- and ARROW-junction) the identification results are shown

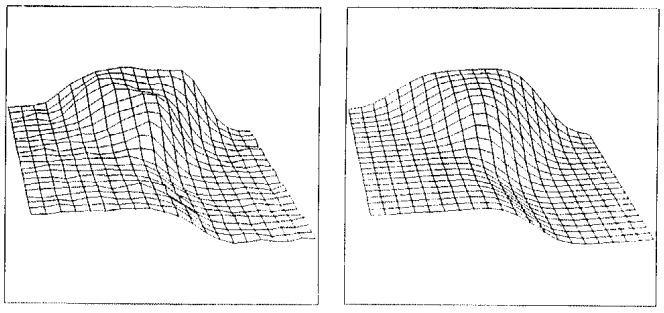

*Figure 22 (left). Original Y-junction*

*Figure 23 (right). Identified model of the Y-junction in Figure 22*

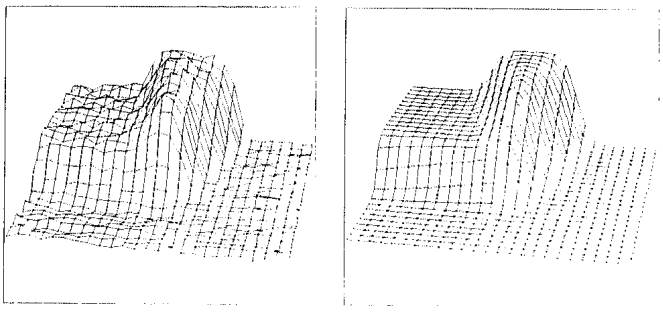

*Figure 24 (left). Original ARROW-junction*

*Figure 25 (right). Identified model of the ARROW-junction in Figure 24*

**Table 3. Identification result of the Y-junction in Figure 22**

| $\sigma_F$ | $x_0$ | $y_0$ | $\alpha$ | $\beta_1$ | $\beta_2$ | $a_0$ | $a_1$ | $a_2$ | $\sigma$ | $\bar{e}$ | $\sigma_0$ |
|---|---|---|---|---|---|---|---|---|---|---|---|
| 0.0 | 29.60 | 26.30 | 91.42 | 59.31 | 146.00 | 124.41 | 177.50 | 59.66 | 1.46 | 2.87 | 1.46 |
| 0.5 | 29.65 | 26.25 | 91.19 | 58.88 | 145.40 | 124.32 | 177.97 | 59.82 | 1.55 | 2.41 | 1.46 |
| 1.0 | 29.69 | 26.20 | 91.17 | 58.70 | 144.56 | 124.09 | 179.05 | 59.66 | 1.87 | 1.69 | 1.58 |
| 1.5 | 29.68 | 26.23 | 91.30 | 58.50 | 145.17 | 124.15 | 179.72 | 59.38 | 2.18 | 1.15 | 1.58 |

**Table 4. Identification result of the ARROW-junction in Figure 24**

| $\sigma_F$ | $x_0$ | $y_0$ | $\alpha$ | $\beta_1$ | $\beta_2$ | $a_0$ | $a_1$ | $a_2$ | $\sigma$ | $\bar{e}$ | $\sigma_0$ |
|---|---|---|---|---|---|---|---|---|---|---|---|
| 0.0 | 21.85 | 32.00 | 230.15 | 68.53 | 31.01 | 12.93 | 42.10 | 69.01 | 1.00 | 2.47 | 1.00 |
| 0.5 | 21.84 | 32.03 | 229.80 | 67.36 | 31.16 | 12.88 | 42.15 | 69.10 | 1.10 | 2.15 | 0.98 |
| 1.0 | 21.82 | 32.13 | 228.58 | 64.14 | 31.43 | 12.76 | 42.30 | 69.10 | 1.40 | 1.73 | 0.97 |
| 1.5 | 21.77 | 32.16 | 228.51 | 63.56 | 31.45 | 12.76 | 42.34 | 68.95 | 1.72 | 1.41 | 0.83 |

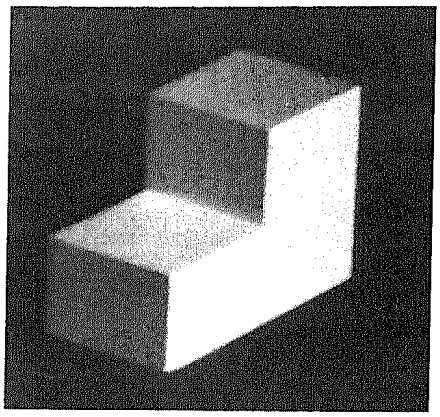

*Figure 26. Original image*

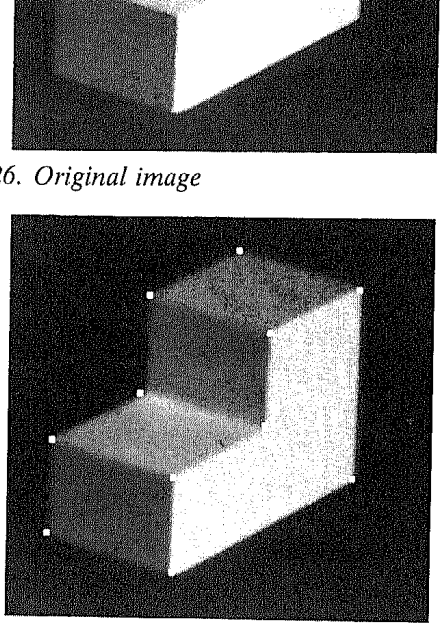

*Figure 27. Detected features of Figure 26*

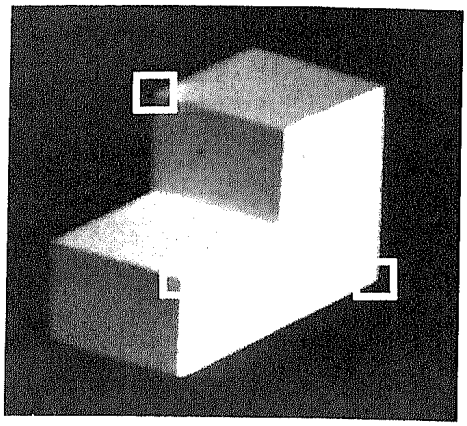

*Figure 28. Considered features of Figure 26*

in Tables 5, 6 and 7. Again, these examples illustrate the properties of our approach mentioned above.

## CONCLUSION AND FUTURE WORK

We have proposed an approach for the modelling and identification of a certain class of characteristic intensity variations. Although the underlying assumptions of the model class (see the first section) seem to be very restrictive, most existing approaches make implicit use of them producing inaccurate results when the assumptions are not met in the image. For modelling this class of intensity variations, we have derived a parametric model which is the superposition of elemen-

**Table 5. Identifcation result of the L-junction in Figure 28**

| $\sigma_F$ | $x_0$ | $y_0$ | $\alpha$ | $\beta$ | $a_0$ | $a$ | $\sigma$ | $\bar{e}$ | $\sigma_0$ |
|---|---|---|---|---|---|---|---|---|---|
| 0.0 | 166.68 | 204.87 | 147.51 | 121.78 | 15.28 | 136.19 | 1.47 | 3.21 | 1.47 |
| 0.5 | 166.69 | 204.86 | 147.40 | 122.06 | 15.29 | 136.20 | 1.55 | 2.86 | 1.47 |
| 1.0 | 166.74 | 204.78 | 146.98 | 123.37 | 15.17 | 136.35 | 1.81 | 2.02 | 1.51 |
| 1.5 | 166.77 | 204.79 | 147.04 | 123.23 | 14.81 | 136.57 | 2.13 | 1.52 | 1.51 |

**Table 6. Identification result of the Y-junction in Figure 28**

| $\sigma_F$ | $x_0$ | $y_0$ | $\alpha$ | $\beta_1$ | $\beta_2$ | $a_0$ | $a_1$ | $a_2$ | $\sigma$ | $\bar{e}$ | $\sigma_0$ |
|---|---|---|---|---|---|---|---|---|---|---|---|
| 0.0 | 165.51 | 99.45 | 329.67 | 118.64 | 104.40 | 93.72 | 138.92 | 54.22 | 1.50 | 2.32 | 1.50 |
| 0.5 | 165.50 | 99.45 | 329.83 | 118.63 | 104.05 | 93.69 | 138.91 | 54.36 | 1.58 | 2.11 | 1.49 |
| 1.0 | 165.51 | 99.43 | 330.52 | 118.67 | 103.99 | 93.48 | 138.78 | 54.72 | 1.82 | 1.60 | 1.52 |
| 1.5 | 165.53 | 99.43 | 330.56 | 118.70 | 104.22 | 93.47 | 139.00 | 54.38 | 2.14 | 1.20 | 1.52 |

**Table 7. Identification result of the ARROW-junction in Figure 28**

| $\sigma_F$ | $x_0$ | $y_0$ | $\alpha$ | $\beta_1$ | $\beta_2$ | $a_0$ | $a_1$ | $a_2$ | $\sigma$ | $\bar{e}$ | $\sigma_0$ |
|---|---|---|---|---|---|---|---|---|---|---|---|
| 0.0 | 59.13 | 83.62 | 2.55 | 48.05 | 68.96 | 11.31 | 83.10 | 56.70 | 1.24 | 1.48 | 1.24 |
| 0.5 | 59.12 | 83.64 | 2.33 | 48.42 | 68.83 | 11.34 | 83.13 | 56.53 | 1.34 | 1.26 | 1.24 |
| 1.0 | 59.08 | 83.66 | 1.87 | 48.99 | 68.17 | 11.36 | 83.10 | 56.18 | 1.63 | 0.90 | 1.29 |
| 1.5 | 59.05 | 83.68 | 1.77 | 48.83 | 68.15 | 11.27 | 83.48 | 56.35 | 1.97 | 0.68 | 1.28 |

tary model functions. By this it is possible to describe step edges, grey-value corners (L-junctions) T-, Y-, ARROW-junctions and all other junction types represented in the labelling system of Waltz[1]. Each grey-value structure can be expressed by just one analytical function and is a special case of the proposed general model. The identification of real intensity variations is done by minimizing the squared difference between the image intensities and the model. By this, we have a measure of how well the estimated model describes the actual data. All parameters can be assigned real values. So the position of the prominent point is determined up to subpixel accuracy and indicates the origin of the ideal (unsmoothed) grey-value structure. We also obtain a measure for the width of the grey-value transitions. Moreover, the estimated parameters are (nearly) independent of smoothing the original image beforehand in order to reduce the noise. The application of the proposed method to real image data demonstrates that the identified model functions agree fairly well with the original grey-value structures. Because of the relatively large size of the grey-value structures being considered (approximately $20 \times 20$ pixels), the approach is computationally expensive. But, in our opinion, it is necessary to examine such large neighbourhoods of each grey-value structure in order to restore prominent features with high accuracy. The high precision we achieve with our approach should increase the reliability of evaluated properties of the 3D-scene and should consequently justify the greater cost. Reducing the computation time will be the subject of future work. One possibility is to perform the algorithm within a pyramid structure of images. A possible extension of our work is the utilization of linearly increasing (descending) grey-value plateaus instead of constant plateaus. Another generalization could be the modelling of curved edges joining in the prominent point of the grey-value structure.

## ACKNOWLEDGEMENTS

I thank H.-H. Nagel for his suggestion to take a high resolution image of a T-junction and for his idea to extend the model of the grey-value corner in Figure 2 to the model of the T-junction in Figure 5. I thank C. Schnörr and J. Rieger for many inspiring discussions and for their help in a variety of ways. Valuable critical comments by G. Hager, A. Korn, H.-H. Nagel, J. Rieger, C. Schnörr and the two referees on a draft version of this contribution are gratefully acknowledged. C. Müller helped me in providing Figure 13.

## REFERENCES

1 **Waltz, D** 'Understanding line drawings of scenes with shadows', in **Winston, P H (ed)**, *The Psychology of Computer Vision*, McGraw-Hill, New York (1975) pp 19–91

2 **Nagel, H-H** 'Wissensgestützte Ansätze beim maschinellen Sehen: Helfen sie in der Praxis?' in **Brauer, W and Radig, B (eds)**, *Wissensbasierte Systeme*, GI – Fachkongreß München, (Germany 28–29 October 1985) pp 170–198

3 **Canny, F** 'A computational approach to edge detection', *IEEE Trans. PAMI* Vol 8 (1986) 679–698

4 **Li, D, Sullivan, G D and Baker, K D** 'Edge detection at junctions', *Proc. 5th Alvey Vision Conf.*, Reading, UK (25–28 September 1989) pp 121–125

5 **Lowe, D G** 'Organization of smooth image curves at multiple scales', *Int. J. Comput. Vision*, Vol 3 (1989) pp 119–130

6 **Damon, J** *Local Morse Theory for Solutions to the Heat Equation*, Preliminary Announcement, Department of Mathematics, University of North Carolina (1989)

7 **Bergholm, F** 'Edge focusing', *IEEE Trans. PAMI*, Vol 9 (1987) pp 726–741

8 **Bergholm, F** *On the Content of Information in Edges and Optical Flow*, Dissertation, Royal Institute of Technology Stockholm, Sweden (May 1989)

9 **Clowes, M** 'On seeing things', *Artif. Intell.*, Vol 2 No 1 (1971) pp 79–116

10 **Huffman, D** 'Impossible objects as nonsense sentences, in **Meltzer, B and Michie, D (eds)**, *Machine Intelligence 6*, Edinburgh University Press, Scotland (1971) pp 295–323

11 **Nagel, H-H** 'Displacement vectors derived from second-order intensity variations in image sequences', *Comput. Vision, Graph. & Image Process.*, Vol 21 (1983) pp 85–117

12 **Dreschler, L and Nagel, H-H** 'Volumetric model and 3D-trajectory of a moving car derived from monocular TV-frame sequences of a street scene', *Proc. IJCAI.* Vancouver, BC (1981) pp 692–697 (see also *Comput. Graph. & Image Process.*, Vol 20 (1982) pp 199–228)

13 **Kitchen, L and Rosenfeld, A** 'Gray-level corner detection', *Patt. Recogn. Lett.*, Vol 1 (1982) pp 95–102

14 **Zuniga, O A and Haralick, R M** 'Corner detection using the facet model', *Proc. IEEE Conf. on Comput. Vision & Patt. Recogn.*, Washington DC (June 19–23 1983) pp 30–37

15 **Noble, J A** 'Finding corners', *Proc. 3rd Alvey Vision Conf.* Cambridge, UK (15–17 September 1987) pp 267–274

16 **Noble, J A** 'Morphological feature detection', *Proc. 4th Alvey Vision Conf.*, Manchester, UK (31 August–2 September 1988) pp 203–210

17 **Rangarajan, K, Shah, M and Van Brackle, D** 'Optimal corner detector', *Comput. Vision, Graph. & Image Process.*, Vol 48 (1989) pp 230–245

18 **Marr, D** 'Early processing of visual information', *Phil. Trans. Royal Soc. London. B*, Vol 275 ( Biol. Sciences) (1976) pp 483–519

19 **Berzins, V** 'Accuracy of Laplacian edge detectors', *Comput. Vision, Graph. & Image Process.*, Vol 27 (1984) pp 195–210

20 **Guiducci, A** 'Corner characterization by differential geometry techniques', *Patt. Recogn. Lett.*, Vol 8 (1988) pp 311–318

21 **Marr, D and Hildreth, E** 'Theory of edge detection', *Proc. Royal Soc. Lond. B* Vol 207 (1980) pp 187–217

22 **Dreschler, L** *Ermittlung markanter Punkte auf den Bildern bewegter Objekte und Berechnung einer 3D-Beschreibung auf dieser Grundlage*, Dissertation, Universität Hamburg, Germany (1981)

23 **Nagel, H-H** 'Principles of (low-level) computer

vision', in **Haton, J-P (ed)**, *Fundamentals in Computer Understanding: Speech and Vision*, Cambridge University Press, UK (1987) pp 113–139

24 **Wolf, H** *Lineare Systeme und Netzwerke*, Springer-Verlag, Berlin (1985)

25 **Press, W H, Flannery, B P, Teukolsky, S A and Vetterling, W T** *Numerical Recipes*, Cambridge University Press, UK (1988)

26 **Abramowitz, M and Stegun, I A** *Handbook of Mathematical Functions*, Dover Publications, New York (1965)

27 **De Micheli, E, Caprile, B, Ottonello, P and Torre V** 'Localization and noise in edge detection', *IEEE Trans. PAMI*, Vol 11 (1989) pp 1106–1117

28 **Norton, J P** *An Introduction to Identification*, Academic Press, London (1986)

29 **Hager, G** *Computational Methods for Sensor Data Fusion and Sensor Planning*, Kluwer, Boston (1990)

30 **Powell, M J D** 'An efficient method for finding the minimum of a function of several variables without calculating derivatives', *Comput. J.*, Vol 7 (1964) 155–162

31 **Rohr, K** *Über die Modellierung und Identifikation charakteristischer Grauwertverläufe in Realweltbildern, 12. DAGM – Symposium Mustererkennung* (24–26 September 1990) *Oberkochen-Aalen, Informatik-Fachberichte 254*, **Großkopf, RE (ed)**, Springer-Verlag, Berlin (1990) pp 217–224

32 **Rohr, K** *Untersuchung von grauwertabhängigen Transformationen zur Ermittlung des optischen Flusses in Bildfolgen*, Diplomarbeit, Institut für Nachrichtensysteme, Universität Karlsruhe, Germany (1987)

33 **Nagel, H-H** 'Constraints for the estimation of displacement vector fields from image sequences', *Proc. IJCAI*, Karlsruhe, Germany (8–12 August 1983) pp 945–951

34 **Nagel, H-H and Enkelmann, W** 'Iterative estimation of displacement vector fields from TV-frame sequences', *Proc. 2nd Euro. Signal Process. Conf.: EUSIPCO-83*, Erlangen, Germany (1983) pp 299–302

35 **Beaudet, P R** 'Rotationally invariant image operators', *Proc. Int. Joint Conf. on Pattern Recogn.*, Kyoto, Japan (November 7–10 1978) pp 579–583

36 **Korn, A** 'Towards a symbolic representation of intensity changes in images', *IEEE Trans. PAMI*, Vol 10 (1988) pp 610–625

37 **Bergholm, F and Rohr, K** *A Comparison between Two Approaches Applied for Estimating Diffuseness and Height of Step Edges*, Hausbericht Nr. 10262, Fraunhofer-Institut für Informations- und Datenverarbeitung (IITB), Karlsruhe, Germany (March 1991)

38 **Zhang, W and Bergholm, F** *An extension of Marr's 'signature' based edge classification*, Technical Note, CVAP-TN04, Department of Numerical Analysis and Computing Science, Royal Institute of Technology, Stockholm, Sweden (September 1990)

39 **Nalwa, V S and Binford, T O** 'On detecting edges', *IEEE Trans. PAMI*, Vol 8 No 6 (1986) pp 699–714